Evaluating the plasmon-exciton interaction in ZnO tetrapods coupled with gold nanostructures by nanoscale cathodoluminescence

IOP Publishing Nano Express 2 (2021) 014004 https://doi.org/10.1088/2632-959X/abe277

NANO EXPRESS

PAPER

Evaluating the plasmon-exciton interaction in ZnO tetrapods coupled with gold nanostructures by nanoscale cathodoluminescence

M Villani[1], F Rossi[1], D Calestani[1], G Salviati[1] and F Fabbri[2,*]

[1] IMEM-CNR, Area delle Scienze 37A, 43124 Parma, Italy
[2] NEST, Istituto Nanoscienze—CNR, Scuola Normale Superiore, Piazza San Silvestro 12, 56127 Pisa, Italy
* Author to whom any correspondence should be addressed.

E-mail: filippo.fabbri@nano.cnr.it

Keywords: cathodoluminescence, plasmon-exciton interaction, photoluminescence, gold nanostructures, ZnO tetrapod

Supplementary material for this article is available online

OPEN ACCESS

RECEIVED
9 December 2020

REVISED
25 January 2021

ACCEPTED FOR PUBLICATION
2 February 2021

PUBLISHED
10 February 2021

Abstract

Plasmon-exciton coupling is gaining increasing interest for enhancing the performance of optoelectronic, photonic and photo-catalytic devices. Herein we evaluate the interaction of excitons in zinc oxide tetrapods with surface plasmons of gold nanostructures with different morphologies. The gold nanostructures are grown *in situ* on ZnO tetrapods by means of a photochemical process, resulting in clean interfaces. The modification of the synthesis parameters results in different morphologies, as isolated nanoparticles, nano-domes or nanoparticles aggregates. Plasmon-exciton interaction is evaluated by means of cathodoluminescence spectroscopy and mapping at the nanoscale. The ZnO excitonic emission is strongly blue-shifted and broadened in close proximity of the gold nanostructures. This effect is explained by the formation of a Schottky barrier that is strongly mediated by the morphology of metal nanostructures.

Introduction

Exciton–plasmon coupling (plexcitons), arise from the coupling between two types of quasiparticles, plasmons and excitons and originates from the Coulomb interaction between the dipole moments of the excitons and the electromagnetic field of surface plasmons [1–3].

Plexcitons can also be categorized, according to the strength of the coupling, into weak and strong interaction regimes [4, 5]. In the weak coupling regime, the wave functions of excitons and plasmons are unperturbed, resulting in the enhanced absorption cross-section [6, 7], increased radiative emissions [7, 8], and exciton–plasmon energy transfers [9, 10]. The strong coupling occurs when the strength of the plasmon–exciton interaction becomes dominant with respect to the damping dissipation in the system [4].

The interaction of localized surface plasmon resonance (LSPR) of metal nanostructures and excitons has been employed to enhanced the optical [11–15] and photonic[16, 17] performances of devices based on different class of materials and nanostructures.

In case of metal oxide nanostructures coupled with metal nanostructures, multiple applications, as SERS bio-sensing [18], chemo-sensing of hazardous species [19], H_2 production [20], UV or near infrared photo-detection [21, 22] and photovoltaics [23, 24] have taken advantage of the plexcitonic properties.

In this work we investigate the plasmon-exciton interaction in ZnO tetrapods coupled with gold nanostructures with different morphologies. To minimize artifacts at the metal/semiconductor interface, the *in situ* photochemical nucleation/growth has been employed. This approach allows to obtain gold nanostructures with different morphologies, to avoid the use of surfactants or of shape controlling molecules and, overall, to obtain clean interfaces. The interaction between the gold nanostructures plasmon and ZnO exciton is evaluated by cathodoluminescence spectroscopy and mapping, carried out at the nanoscale, in a transmission electron microscope. The ZnO excitonic UV emission is strongly blue-shifted and broadened in close proximity of the gold nanostructures and the plasmon light emission is funneled. This effect can be

explained considering an energy transfer from ZnO to gold nanostructures that is strongly mediated by the effective contact surface of the metal nanostructures, possibly due to the formation of a localized Schottky barrier.

Experimental

Zinc Oxide tetrapods (ZnO TP) growth takes advantage of a continuous reaction in a tubular furnace as described elsewhere [25], and up to a few grams of these nanostructures can be obtained in a laboratory scale reactor. The four branches are generally single crystals, growing along the 001 crystallographic direction (the polar axis of the wurtzite structure), and occasionally present zinc blende inclusions [26]. The decoration of ZnO TP with gold nanostructures is based on a modification of a previously reported procedure [18, 27]. Briefly, 10 mg of ZnO TP are added to a 250 ml Erlenmeyer flask together with 100 ml isopropyl alcohol (IPA) and sonicated until an homogeneous dispersion is obtained. The resulting mixture is transferred to a 150 ml becher and proper aliquots of the $HAuCl_4$ precursor dissolved in methanol are injected upon illumination (150 W Osram Solar Simulator lamp) depending of the desired Au morphology:

1. Synthesis of Au nanoparticles (AuNPs): an aliquot consisting of 100 ul of a 0.02% (w/w) solution of $HAuCl_4$ in methanol, is added to the ZnO TP mixture every 10 min, for 20 times.
2. Synthesis of Au nano-domes (AuNDs): an aliquot consisting of 100 ul of a 0.5% (w/w) solution of $HAuCl_4$ in methanol, is added to the ZnO TP mixture every 10 min, for 20 times.
3. Synthesis of Au nanoparticles aggregates (AuNAs): 2 ml of a 0.5% (w/w) solution of $HAuCl_4$ in methanol is added all at once to the ZnO TP mixture.

Room-temperature photoluminescence investigation is carried out using a custom-built, far-field epifluorescence apparatus using a 266 nm laser as the excitation source. The excitation laser was focused by a microscope objective (numerical aperture 0.65) to a 30 μm spot on ZnO nanostructures dispersed onto a carbon tape film. Photoluminescence spectra is recorded through a 300 mm spectrometer (150 lines mm^{-1} grating) using a liquid-nitrogen-cooled CCD (charge-coupled device) detector [28].

STEM-CL measurements were carried out on a JEOL JEM-2011 equipped with a commercial Gatan MonoCL3 system [29, 30] at an accelerating voltage of 120 keV and a spot size of 1.5 nm. The STEM-CL spectra of different samples under analysis were acquired at the same magnification (200 k) and beam current (3 nA).

In order to obtain the size distribution, we measured 243 nanoparticles, 157 nanodomes and 137 nanoaggregates from the STEM images.

Results and discussion

Figure 1(a) resumes the photochemical approach for the synthesis of gold nanostructures of gold nanostructure with different morphologies. The Au particles were synthesized taking advantage of the *in situ* photo-reduction of a gold precursor ($HAuCl_4$) on ZnO TP, without the need of any capping or reducing agents (details are provided in the methods section).

Different gold nanostructures can be obtained by varying the local $HAuCl_4$ supersaturation over time, such as AuNPs, AuNDs or AuNAs.

The different morphology of the obtained gold nanostructures can be explained within the context of the classical La Mer theory of nucleation: going from lower to higher $HAuCl_4$ concentrations increases the local supersaturation to a point where the nucleation and growth stages are no longer separated in time, in this case a homogenous nucleation of Au nuclei onto pre-existing ones' is taking place, leading to gold clustering/nano-aggregates (AuNAs).

Although a quantitative assessment of the influence of local Au^{3+} supersaturation is beyond the scope of the manuscript, a few considerations on the gold nucleation/growth can be deduced. The proposed photo-induced reduction of gold cations is not an equilibrium (i.e. thermodynamic) process: the fast nucleation rate invariably leads to (almost) spherical nuclei (as in the case of AuNP) and not to the equilibrium shapes predicted by the classical Wullf's construction [31] (i.e. minimum energy polyhedron).

Such kinetically limited growth could lead to a flattening of bigger Au particles (e.g. AuNDs), likely due to the nucleation of nanocrystals at ZnO surface reconstruction sites during the early stages of growth, similarly to what was previously observed for the AuNP on TiO_2 [32].

Interestingly by further increasing the gold precursor concentration, it leads to anisotropic Au nano-aggregates (AuNA). Having such structures usually requires seed-mediated growths, co-doping (e.g. Ag^+ ions)

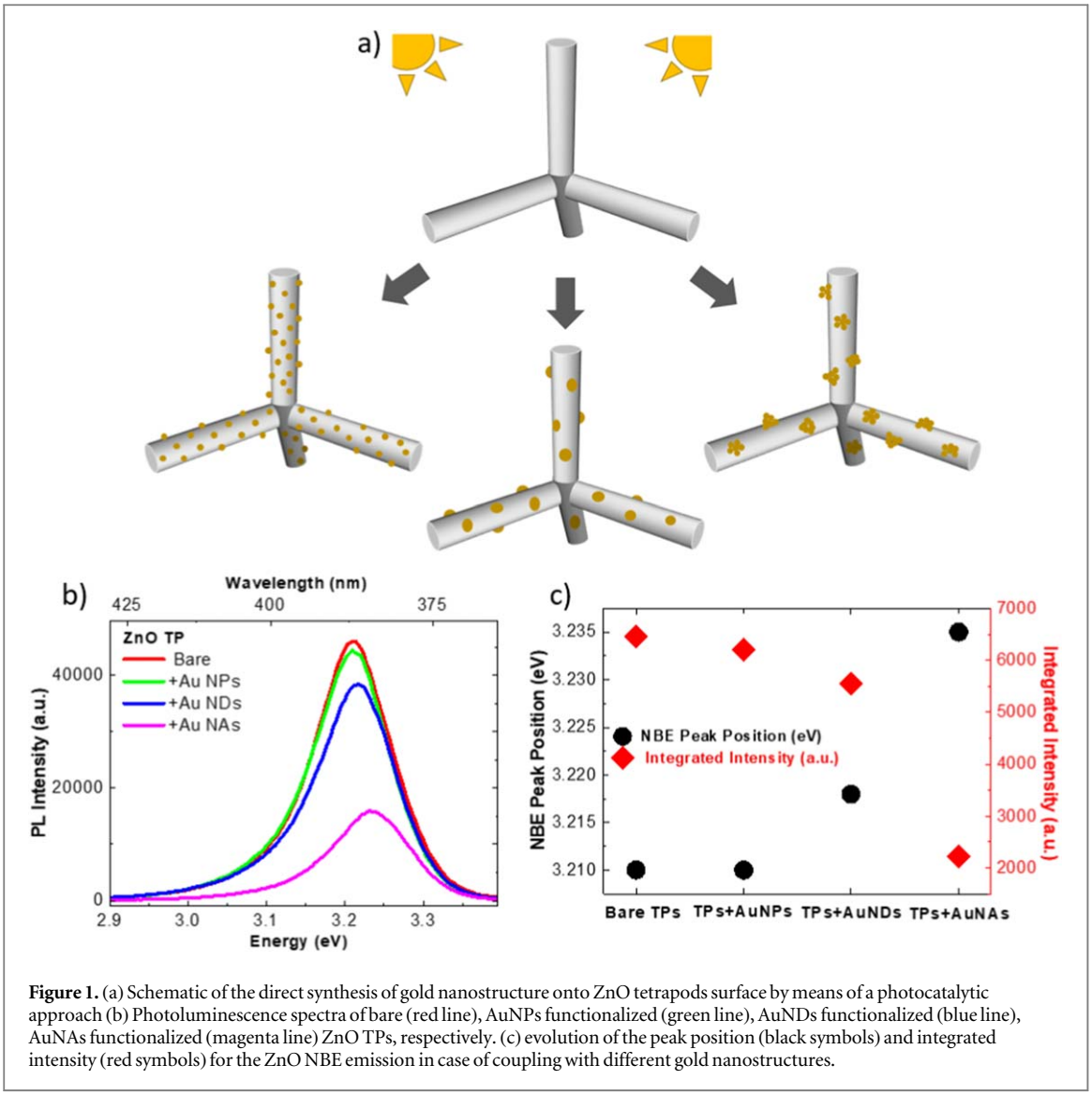

Figure 1. (a) Schematic of the direct synthesis of gold nanostructure onto ZnO tetrapods surface by means of a photocatalytic approach (b) Photoluminescence spectra of bare (red line), AuNPs functionalized (green line), AuNDs functionalized (blue line), AuNAs functionalized (magenta line) ZnO TPs, respectively. (c) evolution of the peak position (black symbols) and integrated intensity (red symbols) for the ZnO NBE emission in case of coupling with different gold nanostructures.

[33, 34] and shape controlling agents (e.g. CTAB, PVP) [35, 36] since the highly symmetric, face-centred cubic (fcc) structure favors the formation of platonic polyhedral as equilibrium shape. Figure 1(b) shows the photoluminescence (PL) spectra of the ZnO TPs coupled with the different gold nanostructures. The PL analysis reports the excitonic near-band-edge emission (NBE) of ZnO, peaked at 3.21 eV (386.3 nm) in case of bare TPs (red line) [28]. The main effect of the coupling with gold nanostructures with different morphologies is a clear blue-shift and a quenching of the NBE emission of ZnO. In particular, as resumed in figure 1(c), the ZnO NBE emission when coupled with AuNPs is peaked at 3.21 eV (386.3 nm), similarly to bare TPS, and the integrated intensity is 96% of the bare ZnO TPs; the blue-shift (0.008 eV) and quenching (86% with respect to the bare TPs emission) are enhanced in case of the coupling with AuNDs, and they are maximized when the ZnO TPs are coupled with AuNAs, with a blue shift of 0.025 eV and an intensity of 35% of the bare TPs NBE emission. A similar effect was previously reported in case of gold nanoparticles assisted synthesis of ZnO nanowires [28]. It is worth noting that the PL spectra of all the TP, both bare and coupled with metal nanostructures, do not present any light emission in the visible range, related to ZnO point-defects or to localized surface plasmon resonance (LSPR) of metal nanostructures. (See supporting Information Figure S1 (available online at stacks.iop.org/NANOX/2/014004/mmedia)).

Figure 2 presents the STEM-CL analysis of the bare ZnO TP. In particular figures 2(a) and (b) present the STEM image and the STEM-CL panchromatic map of a single TP. The three TP branches on the same plane present a similar CL emission intensity; meanwhile the vertical branch presents an enhanced emission due to vertical orientation of the branch, therefore an artifact due to the geometry of the tetrapod and of the CL acquisition mirror. It is worth noting that the core of the TP presents a faint emission, related to the non-radiative recombination at extended defects like stacking faults (SFs) at the boundaries between the arms (wurtzite/wurtzite interface with a twin relationship [37] which can cause the quenching of the NBE emission of

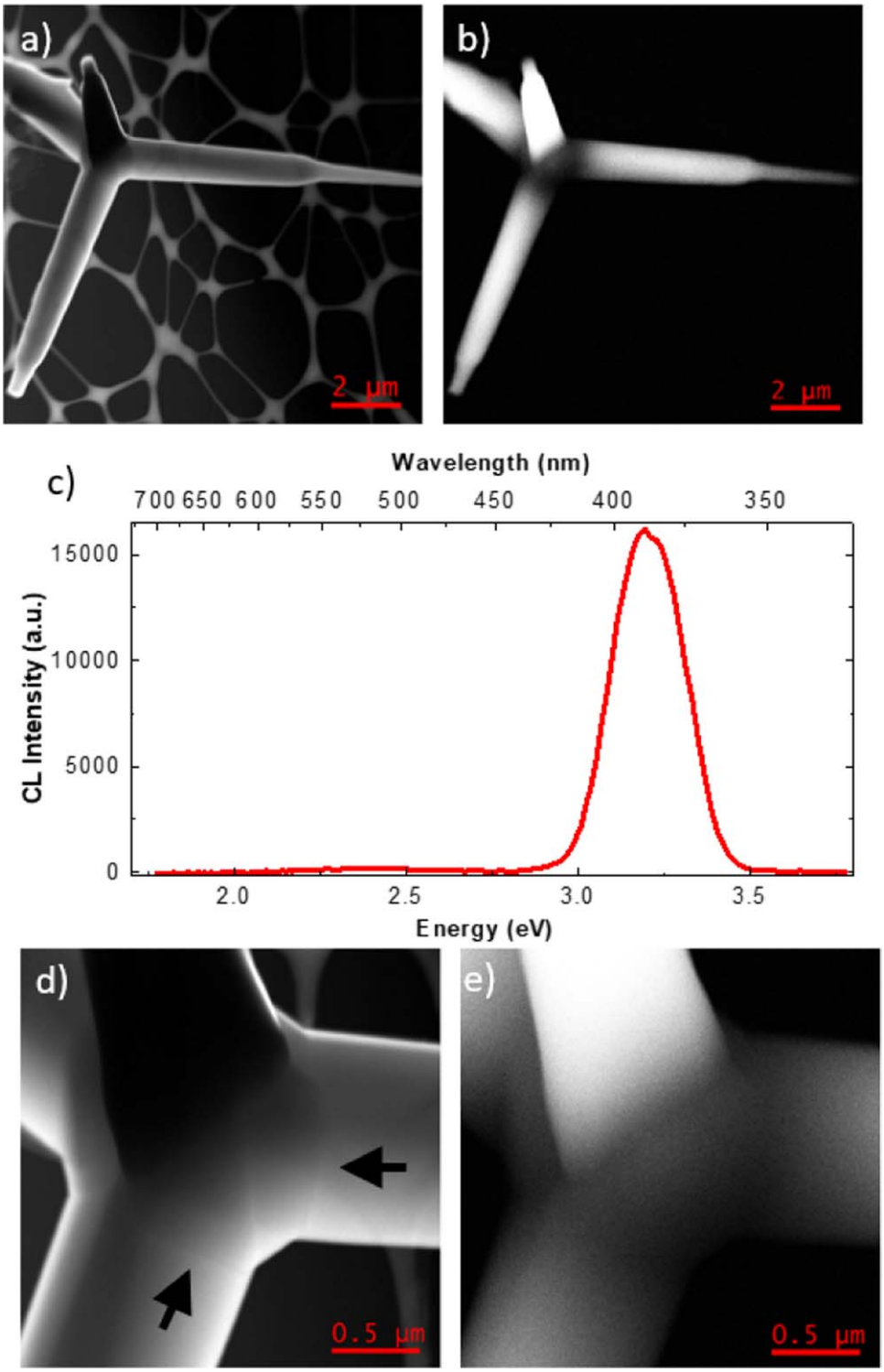

Figure 2. (a) and (b) STEM image and panchromatic CL map of bare ZnO tetrapods, respectively (c) CL spectra of bare ZnO tetrapods (d) and (e) High magnification STEM image and panchromatic CL map of TP core, revealing the presence of extended defects at the base of TP branches.

ZnO. The CL spectrum of the single TP, (figure 2(c)) presents a single peak at 3.20 eV (387 nm) due to the excitonic NBE emission of ZnO. It is worth noting that in bare TP presents a weak emission at 2.42 eV (512 nm) related to the presence of point defects in ZnO. The point defect related emission in ZnO nanostructures are often attributed either to O or Zn vacancy [38–40].

The high magnification STEM image reveals the presence of the extended defects in the TP core and at the interface between the core and branch, as line with a bright contrast, highlighted by black arrows in figure 2(d). The STEM-CL panchromatic map of the same region (figure 2(e)) evaluates the spatial extent of the light emission quenching due to the presence of the extended defects. The light emission quenching spatial extend is

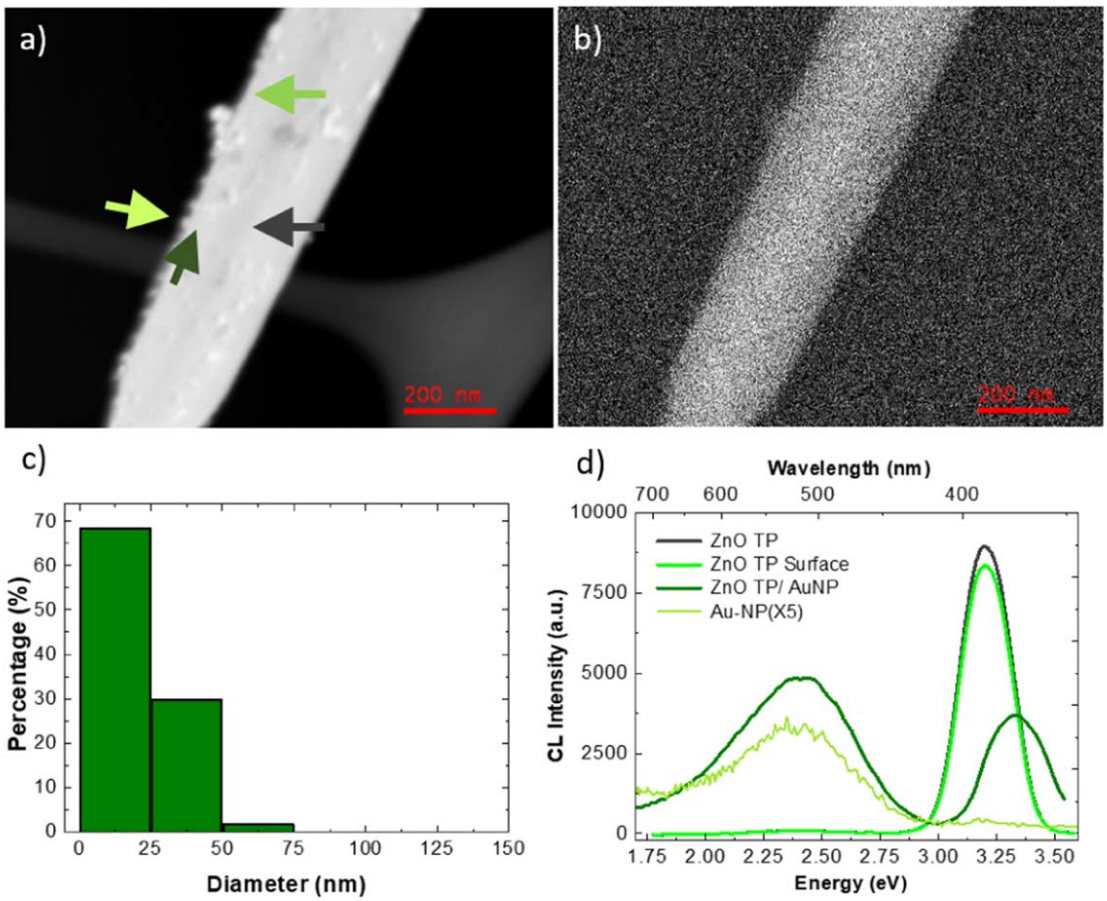

Figure 3. (a) and (b) STEM image and panchromatic CL map of gold nano-particles coupled ZnO tetrapods, respectively (c) AuNPs size distribution obtained by the STEM imaging (d) spot-mode CL spectra of the areas indicated by the colored arrows in panel a (spectra and arrows have the same color code). The spectra acquired on the AuNP is multiplied by 5 for clarity.

about 200 nm along the branch of the TP. A previous work [41] assessed that the TP core can have a zinc blend crystal structure. An accurate comparison of HR-TEM imaging and CL monochromatic mapping of the core structure of TPs revealed the presence of basal-plane SFs and/or twin boundaries (TBs) responsible for nonradiative CL lines [26]. CL spectra of the upper branch, lateral branch and TP core are reported in figure S2 of the Supporting Information.

The STEM image and the STEM-CL map of Au NPs coupled ZnO TP are reported in figures 3(a) and (b), respectively. The STEM image reveals the presence of AuNPs with different diameter ranging from 20 nm up to 70 nm in case of small aggregates. The NPs size distribution is resumed in the histogram reported in figure 3(c). The STEM-CL panchromatic map presents homogeneous light emission intensity along the TP branch. It is worth noting the presence of a faint emission in correspondence of the AuNPs. In order to evaluate the possible decrease of the intensity of the ZnO NBE emission related to the round shape of the tetrapod branch, spot-mode CL spectra have been acquired on the center (grey line) and close to the bare surface of the TP (light green line). The NBE emission is peaked at the same energy and the intensity is slightly decreased (93%) with respect to the spectrum acquired at the center of the branch. The spot-mode CL spectra, acquired in proximity of a gold nanoparticle (dark green line and arrow in figure 3(a)) and on a nanoparticle-free area close to the surface (light green line and arrow in figure 3(a)), reveals that the NBE emission is blue shifted of 0.135 eV. In fact, the NBE emission in NPs free ZnO is set at 3.20 eV (387 nm) and it blue shifts up to 3.335 eV (372 nm) when the spectrum is acquired close to the metal nanostructure. The ZnO NBE emission in proximity of the AuNP presents also a quenching of the 50% of the integrated intensity and a broadening of the FWHM from 0.24 eV up to 0.31 eV. Further, the CL spectrum obtained in close proximity to the AuNP shows a broad band at 2.41 eV (514.5 nm) attributable to the localized plasmon resonance of the metal nanostructures. The spectrum acquired onto the gold nanoparticles (yellow-green line and arrow) presents a weak emission centered at 2.41 eV. (514 nm)

The STEM image and the STEM-CL map of AuNDs coupled ZnO TP are presents in figures 4(a) and (b), respectively. The size of the gold nanodomes can be evaluated by STEM imaging, with a diameter at the base varying from 35 nm up to 110 nm and with a height ranging from 12 nm to 83 nm. It is worth noting that the dark contrast in STEM imaging of nanodomes is due to the low electron transparency related to the

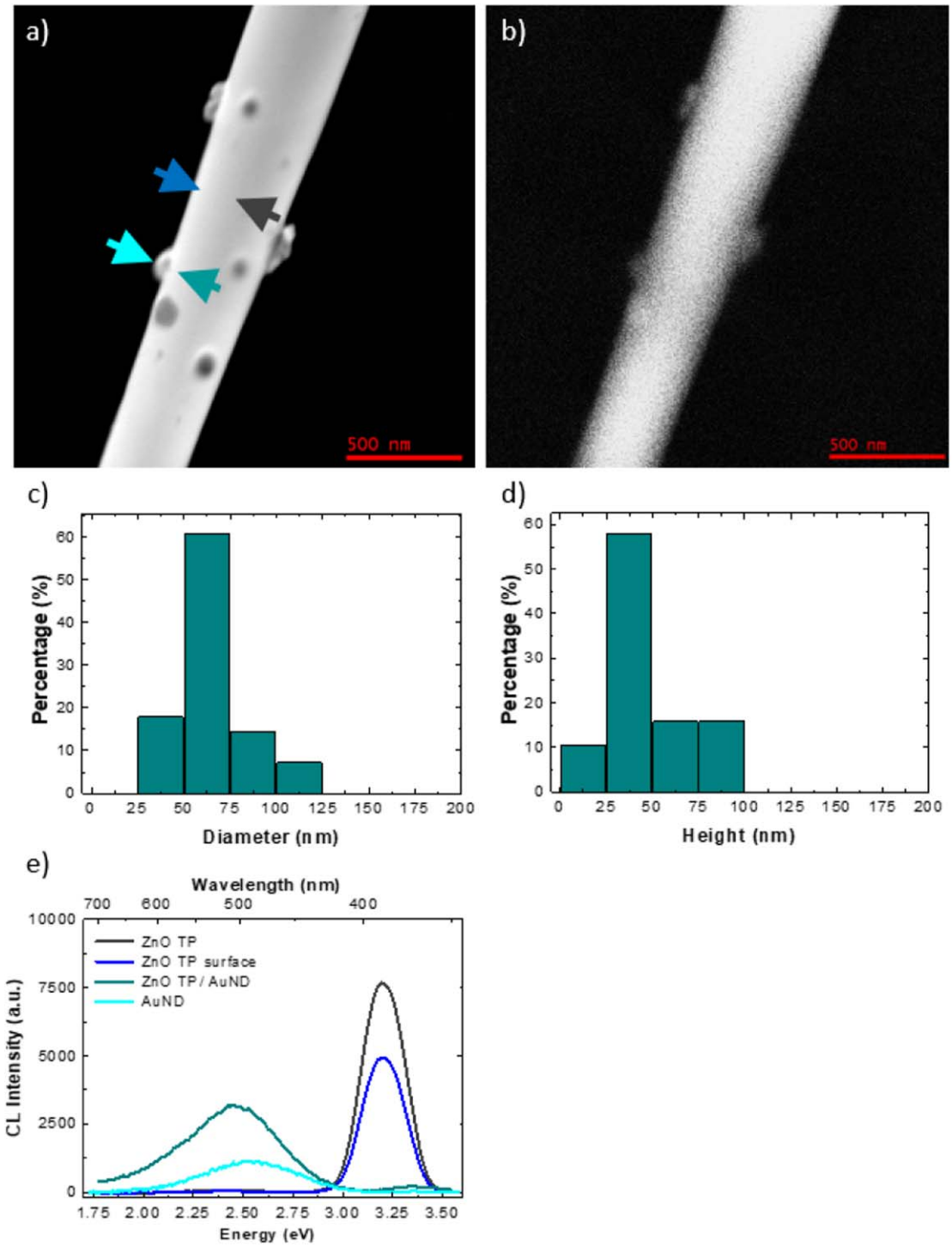

Figure 4. (a) and (b) STEM image and panchromatic CL map of gold nanodomes coupled ZnO tetrapods, respectively (c), (d) AuNDs diameter and height distributions obtained by the STEM imaging, respectively (e) spot-mode CL spectra of the areas indicated by the colored arrows in panel (spectra and arrows have the same color code).

nanostructures sizing and chemical composition. The NDs diameter and height distribution is resumed in the histogram reported in figures 4(c) and (d). The STEM-CL panchromatic map presents homogeneous light emission intensity in bare areas; meanwhile the light emission is quenched in proximity of the gold nanodomes. The AuNDs present a more intense light emission in comparison with gold nanoparticles. In figure 4(e) the spot-mode CL spectra are reported with the same color code of the arrows in figure 4(a). The NBE intensity decrease due to the round shape of the branch is evaluated collecting spot-mode CL spectra on the center (gray line) and on the bare surface (blue line) of the TP. The comparison shows an intensity decrease of the 64%, while being peaked at the same energy. The CL spectra obtained in proximity of a gold nanodome (dark cyan line) and in a bare surface area (blue line), shows that the ZnO NBE emission presents a quite complete quenching (95%

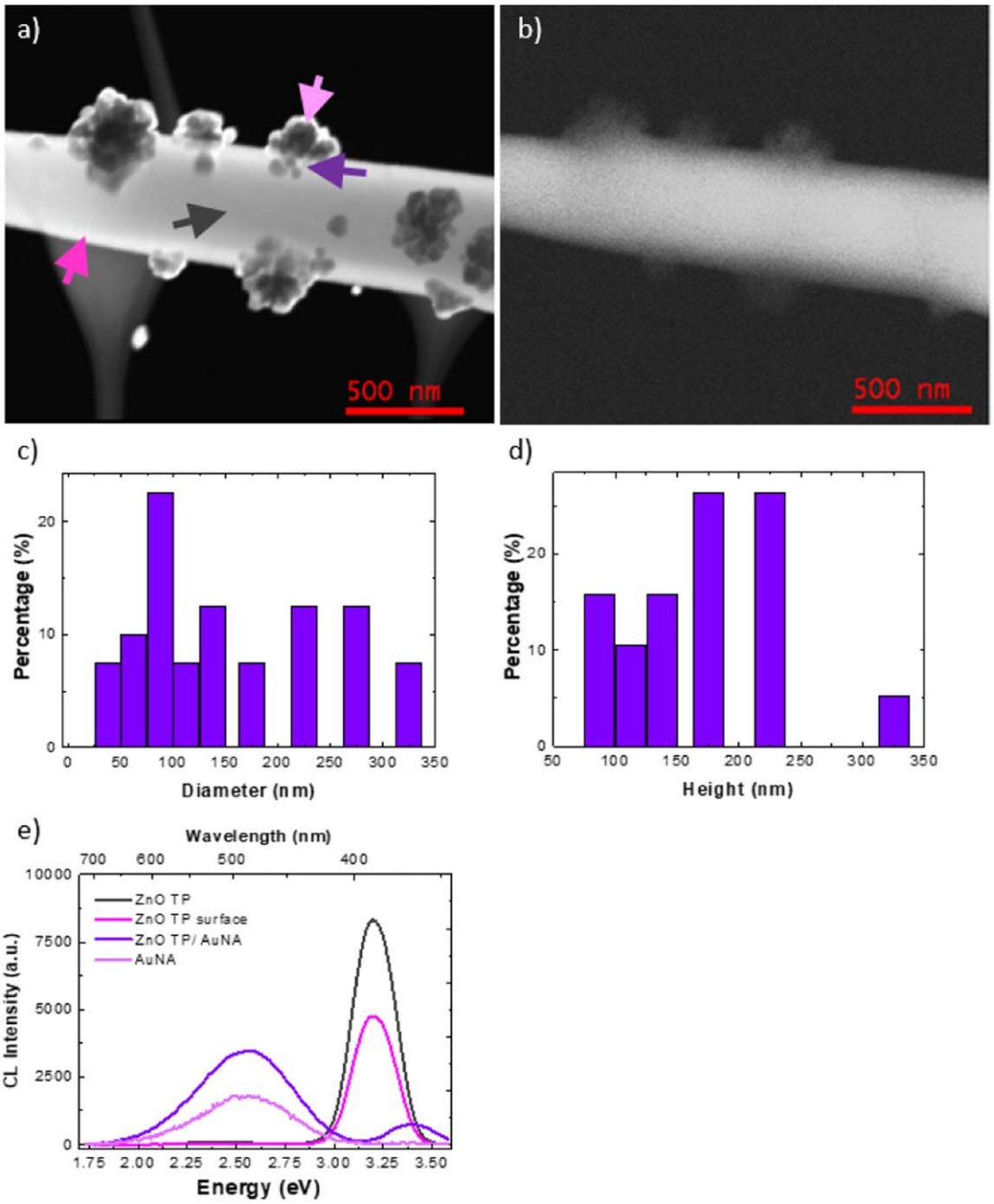

Figure 5. (a) and (b) STEM image and panchromatic CL map of gold nano-aggregates coupled ZnO tetrapods, respectively (c), (d) AuNAs diameter and height distributions obtained by the STEM imaging, respectively (e) spot-mode CL spectra of the areas indicated by the colored arrows in panel (spectra and arrows have the same color code).

compared to the bare surface area) with a concurrent broadening (from FWHM = 0.24 eV up to 0.28 eV) and blue shift of 0.17 eV. In fact, the NBE emission in bare ZnO is peaked at 3.20 eV (387 nm) and it blue-shifts up to 3.37 eV (368 nm) when the spectrum is collected close to the metal nanostructure. The broad emission peaked 2.44 eV (508 nm) is due to the localized plasmon resonance of the gold nanodomes. Noteworthy, the CL spectrum collected onto the AuND presents a blue-shifted emission with similar FWHM. The emission is peaked at 2.55 eV (486 nm). The blue-shift of the LSPR is probably due to the smaller size of the gold nanodomes at the tip where the spectrum is collected [42].

Figures 5(a) and (b) shows the STEM image and the STEM-CL map of ZnO TP coupled with AuNAs, respectively. As in the case of gold nanodomes, also the nano aggregates of nanoparticles have a dark STEM contrast due to the size of the nanostructures. The STEM imaging also shows the coexistence of nano-aggregates with nano-domes. The STEM panchromatic CL map reveals that the light emission is homogeneous along the TP branch, except for the areas close to the nanoaggregates, where the luminescence is slightly quenched. The nanoaggregates present a faint luminescence. The distributions of the nano-aggregates diameter and height are

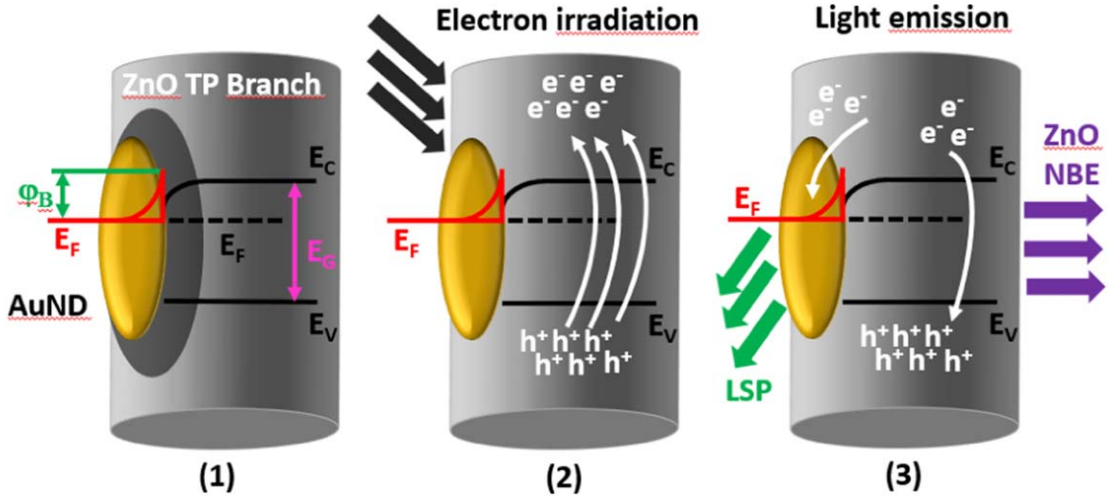

Figure 6. Sketch of the effect of the metal nanostructure coupling with ZnO TP. Step 1: the formation of a localized Schottky barrier between gold and ZnO with related depletion region (dark shadow) ; step 2 the electron irradiation creates electron-hole couples where the electrons are excited in higher conduction band states of ZnO; step 3: thermalization process, part of the electrons are driven toward the metal nanostructures funneling the light emission of the localized surface plasmon, while part of the electrons thermalize in the conduction band of ZnO.

reported in figures 5(c) and (d), respectively. The Au-NA diameter varies from 30 nanometers up to 320 nm, meanwhile the height ranges from 80 nm up to 320 nm. The comparison of the spot-mode CL spectra collected on the branch center (gray line) and close to the branch surface (magenta line) reveals an intensity decrease of the ZnO NBE emission, namely 57%, due to the round shape of the TP, while the peaks is centered at the same energy. The spot-mode CL spectrum obtained in bare surface (magenta line) presents the ZnO NBE peak at 3.20 eV (387 eV) with a FWHM of 0.24 eV, meanwhile the spectrum, acquired in close proximity of the Au-NA (purple line), presents two peaks: the first is positioned at 2.54 eV (488 nm), related to the localized plasmon resonance of the metal nanostructures, the second peak, attributed to ZnO NBE, is centered at 3.39 eV (365.8 nm) with a FWHM of 0.275 eV. The proximity to the gold nanoaggregates causes a blue shift of the ZnO NBE emission of 0.19 eV, a broadening of 0.035 eV and the quenching of the 90% of the integrated intensity in comparison with the peak obtained in the bare ZnO area. The spot-mode CL spectrum collected on the gold nano-aggregate (pink line) presents an emission related to the LSPR, centered at 2.56 eV (484 nm).

Figure 6 depicts the effect of the coupling of metal nanostructures with ZnO tetrapod. The first step sketches the formation a localized Schottky barrier due to the gold nanostructures coupling, as reported in previous works [24, 43–45]. The darker shadow area below the gold nanostructure represents the depletion region caused by the Schottky barrier. The presence of the depletion region is demonstrated by the decrease of the panchromatic emission in close proximity of AuNDs and AuNAs in STEM-CL maps (figures 4(b) and (b)). Step 2 represents the electron excitation during STEM-CL experiments with the concurrent promotion of electrons toward higher conduction band states. Step three represents the thermalization and light emission processes. Part of the generated electrons is driven toward the gold nanostructures, funneling the light emission of the LSPR, while part of the electrons thermalizes toward the minimum of the ZnO conduction band resulting in the NBE emission of ZnO. However, the ZnO NBE blue-shift suggests the existence of a direct electromagnetic interaction between gold nanostructures and the ZnO TP. In particular, the blue-shift of NBE emission in AuNP coupled ZnO nanostructures was previously attributed to the decreasing in the lifetime of the ZnO excitons due to the direct interaction with gold nanostructures LSPR, which does not permit to reach potential minima [13, 27, 46].

It is worth noting that the UV (266 nm, 4.66 eV) excited PL experiments demonstrate that the effect of the metal nanostructures coupling on the NBE emission of ZnO TPs is similar to the CL spectra acquired close to the metal nanostructures except for the funneling of the LSPR emission [28]. This effect is probably due to the lower excitation density of PL experiments compared to CL experiments.

However, we can differentiate the effect of the gold nanostructures depending on the size and morphology. We consider three different effects occurring to the ZnO excitonic NBE emission: (i) the integrated intensity quenching, (ii) the broadening of the emission peak and (iii) the blue-shift of NBE emission. The luminescence quenching is maximized in the case of AuNDs with 97% and it reaches the 90% for AuNAs meanwhile in the case of single gold nanoparticles the quenching is limited to the 53%. The broadening of the NBE emission is maximum in case of AuNP (0.07 eV) and it decreases monotonically in case of AuNDs (0.04 eV) and AuNAs

(0.035 eV). On the contrary the blue-shift of the ZnO NBE emission increases monotonically from 0.135 eV in case of AuNPs up to 0.275 eV for AuNAs, with an intermediate value of 0.17 eV for AuNDs. Even if the AuNAs have larger size in comparison with AuNDs, the quenching is maximized in this latter case; this effect is probably dominated by the efficient interface between gold and ZnO. In fact, the AuNDs have a larger clear interface in comparison with the AuNAs due to a more discontinuous interface with ZnO caused by the polycrystalline nature of the nanostructure. On the contrary, the blue shift of the UV emission is maximized in case of the coupling with the AuNAs; this effect seems to be more dominated by the overall size of the metal nanostructures probably due to the larger amount/thickness of gold deposited on the ZnO surface.

Conclusions

The interaction of excitons in zinc oxide tetrapods with surface plasmons of gold nanostructures—with different morphologies—has been evaluated by nanoscale cathodoluminescence. The gold nanostructures are grown *in situ* on ZnO tetrapods by means of a photochemical process that does not rely on any capping molecule to provide dimensional control, thus resulting in clean interfaces. The modification of the synthesis parameters allows to obtain isolated nanoparticles, nano-domes or nanoparticles aggregates. Plasmon-exciton interaction is evaluated by means of cathodoluminescence spectroscopy and mapping at the nanoscale. The ZnO excitonic emission is strongly affected by the proximity to the gold nanostructures, with a consequent quenching of the integrated intensity, a broadening and a blue-shift of UV the near-band-edge emission, with a concurrent funneling of the LSPR emission. This effect is due to the formation of a Schottky barrier between the gold nanostructures and ZnO. The modification of the ZnO UV emission is strongly dependent on the gold nanostructures morphology. The NBE UV blue-shift is maximized in case of coupling with gold nano-aggregates, meanwhile the coupling with nano-domes enhances the integrated intensity quenching which is strongly mediated by the effective interface between the metal nanostructures and the ZnO surface as a result of the formation of a Schottky barrier.

Acknowledgments

The authors want to thank Prof. Silvija Gradecak (Department of Materials Science & Engineering, National University of Singapore) for the useful discussion about the cathodoluminescence results. The authors would like to acknowledge Dr. S. Chen of the MIT Center of Material Science and Engineering (CMSE) for supporting the STEM-CL measurements.

Data availability statement

The data that support the findings of this study are available upon reasonable request from the authors.

ORCID iDs

M Villani https://orcid.org/0000-0002-9229-3490
F Rossi https://orcid.org/0000-0003-1773-2542
D Calestani https://orcid.org/0000-0003-3344-8007
G Salviati https://orcid.org/0000-0002-9828-6371
F Fabbri https://orcid.org/0000-0003-1142-0441

References

[1] Manjavacas A, García de Abajo F J and Nordlander P 2011 Quantum plexcitonics: strongly interacting plasmons and excitons *Nano Lett.* **11** 2318–23
[2] Sukharev M, Day P N and Pachter R 2015 Optical response of hybrid plasmon–exciton nanomaterials in the presence of overlapping resonances *ACS Photonics* **2** 935–41
[3] Manuel A P, Kirkey A, Mahdi N and Shankar K 2019 Plexcitonics—fundamental principles and optoelectronic applications *J. Mater. Chem. C* **7** 1821–53
[4] Achermann M 2010 Exciton−plasmon interactions in metal−semiconductor nanostructures *J. Phys. Chem. Lett.* **1** 2837–43
[5] Ebner J, Trügler A and Hohenester U 2015 Optical excitations of hybrid metal-semiconductor nanoparticles *Eur. Phys. J. B* **88** 11
[6] Maaroof A I, Lee H, Heo K, Park J, Cho D, Lee B Y, Seong M-J and Hong S 2013 Plasmon–exciton interactions in hybrid structures of Au nanohemispheres and CdS nanowires for improved photoconductive devices *J. Phys. Chem. C* **117** 24543–8
[7] Song J-H, Atay T, Shi S, Urabe H and Nurmikko A V 2005 Large enhancement of fluorescence efficiency from CdSe/ZnS quantum dots induced by resonant coupling to spatially controlled surface plasmons *Nano Lett.* **5** 1557–61

[8] Lee J, Govorov A O, Dulka J and Kotov N A 2004 Bioconjugates of CdTe nanowires and Au Nanoparticles: plasmon−exciton interactions, luminescence enhancement, and collective effects *Nano Lett.* **4** 2323–30

[9] Govorov A O, Lee J and Kotov N A 2007 Theory of plasmon-enhanced F\'orster energy transfer in optically excited semiconductor and metal nanoparticles *Phys. Rev. B* **76** 125308

[10] Hernández-Martínez P L and Govorov A O 2008 Exciton energy transfer between nanoparticles and nanowires *Phys. Rev. B* **78** 35314

[11] Sun J, Hu H, Zheng D, Zhang D, Deng Q, Zhang S and Xu H 2018 Light-emitting plexciton: exploiting plasmon–exciton interaction in the intermediate coupling regime *ACS Nano* **12** 10393–402

[12] Zheng D, Zhang S, Deng Q, Kang M, Nordlander P and Xu H 2017 Manipulating coherent plasmon–exciton interaction in a single silver nanorod on monolayer WSe2 *Nano Lett.* **17** 3809–14

[13] Lawrie B J, Kim K-W, Norton D P and Haglund R F 2012 Plasmon–exciton hybridization in ZnO quantum-well al nanodisc heterostructures *Nano Lett.* **12** 6152–7

[14] Butun S, Palacios E, Cain J D, Liu Z, Dravid V P and Aydin K 2017 Quantifying plasmon-enhanced light absorption in monolayer WS2 films *ACS Appl. Mater. Interfaces* **9** 15044–51

[15] Wang M, Li W, Scarabelli L, Rajeeva B B, Terrones M, Liz-Marzán L M, Akinwande D and Zheng Y 2017 Plasmon–trion and plasmon–exciton resonance energy transfer from a single plasmonic nanoparticle to monolayer MoS2 *Nanoscale* **9** 13947–55

[16] Grinblat G, Rahmani M, Cortés E, Caldarola M, Comedi D, Maier S A and Bragas A V 2014 High-efficiency second harmonic generation from a single hybrid ZnO Nanowire/Au plasmonic nano-oligomer *Nano Lett.* **14** 6660–5

[17] Richter J, Steinbrück A, Zilk M, Sergeyev A, Pertsch T, Tünnermann A and Grange R 2014 Core–shell potassium niobate nanowires for enhanced nonlinear optical effects *Nanoscale* **6** 5200–7

[18] Picciolini S *et al* 2015 Branched gold nanoparticles on ZnO 3D architecture as biomedical SERS sensors *RSC Adv.* **5** 93644–51

[19] Filanovsky B, Markovsky B, Bourenko T, Perkas N, Persky R, Gedanken A and Aurbach D 2007 Carbon electrodes modified with TiO_2/metal nanoparticles and their application for the detection of trinitrotoluene *Adv. Funct. Mater.* **17** 1487–92

[20] Naldoni A, Fabbri F, Altomare M, Marelli M, Psaro R, Selli E, Salviati G and Dal Santo V 2015 The critical role of intragap states in the energy transfer from gold nanoparticles to TiO_2 *Phys. Chem. Chem. Phys.* **17**

[21] Pescaglini A, Martín A, Cammi D, Juska G, Ronning C, Pelucchi E and Iacopino D 2014 Hot-electron injection in Au nanorod–ZnO nanowire hybrid device for near-infrared photodetection *Nano Lett.* **14** 6202–9

[22] Liu K, Sakurai M, Liao M and Aono M 2010 Giant Improvement of the performance of ZnO nanowire photodetectors by Au nanoparticles *J. Phys. Chem. C* **114** 19835–9

[23] Lu Q, Lu Z, Lu Y, Lv L, Ning Y, Yu H, Hou Y and Yin Y 2013 Photocatalytic synthesis and photovoltaic application of Ag-TiO_2 nanorod composites *Nano Lett.* **13** 5698–702

[24] Chen Z H *et al* 2009 Vertically aligned ZnO nanorod arrays sentisized with gold nanoparticles for schottky barrier photovoltaic cells *J. Phys. Chem. C* **113** 13433–7

[25] Villani M, Rimoldi T, Calestani D, Lazzarini L, Chiesi V, Casoli F, Albertini F and Zappettini A 2013 Composite multifunctional nanostructures based on ZnO tetrapods and superparamagnetic Fe3O4nanoparticles *Nanotechnology* **24** 135601

[26] Lazzarini L, Salviati G, Fabbri F, Zha M, Calestani D, Zappettini A, Sekiguchi T and Dierre B 2009 Unpredicted nucleation of extended zinc blende phases in wurtzite ZnO nanotetrapod arms *ACS Nano* **3**

[27] Bertoni G, Fabbri F, Villani M, Lazzarini L, Turner S, Van Tendeloo G, Calestani D, Gradečak S, Zappettini A and Salviati G 2016 Nanoscale mapping of plasmon and exciton in ZnO tetrapods coupled with Au nanoparticles *Sci. Rep.* **6**

[28] Brewster M M, Zhou X, Lim S K and Gradečak S 2011 Role of Au in the growth and nanoscale optical properties of ZnO nanowires *J. Phys. Chem. Lett.* **2** 586–91

[29] Lim S K, Brewster M, Qian F, Li Y, Lieber C M and Gradečak S 2009 Direct correlation between structural and optical properties of III−V nitride nanowire heterostructures with nanoscale resolution *Nano Lett.* **9** 3940–4

[30] Singh A, Lee H Y and Gradečak S 2020 Direct optical-structure correlation in atomically thin dichalcogenides and heterostructures *Nano Res.* **13** 1363–8

[31] Barmparis G D and Remediakis I N 2012 Dependence on CO adsorption of the shapes of multifaceted gold nanoparticles: a density functional theory *Phys. Rev. B* **86** 85457

[32] Sivaramakrishnan S, Wen J, Scarpelli M E, Pierce B J and Zuo J-M 2010 Equilibrium shapes and triple line energy of epitaxial gold nanocrystals supported on TiO2(110) *Phys. Rev. B* **82** 195421

[33] Liu M and Guyot-Sionnest P 2005 Mechanism of silver(I)-assisted growth of gold nanorods and bipyramids *J. Phys. Chem. B* **109** 22192–200

[34] Busbee B D, Obare S O and Murphy C J 2003 An improved synthesis of high-aspect-ratio gold nanorods *Adv. Mater.* **15** 414–6

[35] Pérez-Juste J, Liz-Marzán L M, Carnie S, Chan D Y C and Mulvaney P 2004 Electric-field-directed growth of gold nanorods in aqueous surfactant solutions *Adv. Funct. Mater.* **14** 571–9

[36] Ah C S, Yun Y J, Park H J, Kim W-J, Ha D H and Yun W S 2005 Size-controlled synthesis of machinable single crystalline gold nanoplates *Chem. Mater.* **17** 5558–61

[37] Ding Y, Wang Z L, Sun T and Qiu J 2007 Zinc-blende ZnO and its role in nucleating wurtzite tetrapods and twinned nanowires *Appl. Phys. Lett.* **90** 153510

[38] Djurišić A B *et al* 2007 Defect emissions in ZnO nanostructures *Nanotechnology* **18** 95702

[39] Djurišić A B and Leung Y H 2006 Optical properties of ZnO nanostructures *Small* **2** 944–61

[40] Fabbri F *et al* 2014 Zn vacancy induced green luminescence on non-polar surfaces in ZnO nanostructures *Sci. Rep.* **4**

[41] Newton M C and Warburton P A 2007 ZnO tetrapod nanocrystals *Mater. Today* **10** 50–4

[42] Kociak M and Stéphan O 2014 Mapping plasmons at the nanometer scale in an electron microscope *Chem. Soc. Rev.* **43** 3865–83

[43] Zhang W, Wang W, Shi H, Liang Y, Fu J and Zhu M 2018 Surface plasmon-driven photoelectrochemical water splitting of aligned ZnO nanorod arrays decorated with loading-controllable Au nanoparticles *Sol. Energy Mater. Sol. Cells* **180** 25–33

[44] Park W I, Yi G-C, Kim J-W and Park S-M 2003 Schottky nanocontacts on ZnO nanorod arrays *Appl. Phys. Lett.* **82** 4358–60

[45] Bora T, Kyaw H H, Sarkar S, Pal S K and Dutta J 2011 Highly efficient ZnO/Au schottky barrier dye-sensitized solar cells: role of gold nanoparticles on the charge-transfer process *Beilstein J. Nanotechnol.* **2** 681–90

[46] Chen B, Zhang H, Du N, Li D, Ma X and Yang D 2009 Hybrid nanostructures of Au nanocrystals and ZnO nanorods: layer-by-layer assembly and tunable blue-shift band gap emission *Mater. Res. Bull.* **44** 889–92